Regular Article

Developing advanced models of biological membranes with hydrogenous and deuterated natural glycerophospholipid mixtures

Giacomo Corucci [a,b,1], Krishna Chaithanya Batchu [a,1], Alessandra Luchini [c,d,2],
Andreas Santamaria [a,e,3], Moritz Paul Karl Frewein [a,f], Valèrie Laux [a], Michael Haertlein [a],
Yoshiki Yamaryo-Botté [g], Cyrille Y. Botté [g], Thomas Sheridan [h,i,2], Mark Tully [j],
Armando Maestro [l,k], Anne Martel [a], Lionel Porcar [a], Giovanna Fragneto [a,b,c,*,4]

a Institut Laue-Langevin, 71 avenue des Martyrs, CS 20156, 38042 Grenoble, France
b École doctorale de Physique, Université Grenoble Alpes, 38400 Saint-Martin-d'Héres, France
c European Spallation Source ERIC, P.O. Box 176, SE-221 00 Lund, Sweden
d Department of Physics and Geology, University of Perugia, Via Alessandro Pascoli, 06123 Perugia, Italy
e Departamento de Química Física, Universidad Complutense de Madrid, 28040 Madrid, Spain
f Institute of Molecular Biosciences, University of Graz, NAWI Graz, Graz, 8010, Austria
g ApicoLipid Team & GEMELI Lipidomics Platform, Institute for Advanced Biosciences, CNRS UMR5309, INSERM (-National Institute for Health and Medical Research)
U1209, Université Grenoble Alpes, 38000 Grenoble, France
h University College Dublin, Belfield, Dublin 4, Dublin, Ireland
i AbbVie, Clonshaugh, Dublin 7, Co. Dublin, Ireland
j European Synchrotron Radiation Facility (ESRF), 71 avenue des Martyrs, CS 40220, 38043, Grenoble, France
k Centro de Física de Materiales (CSIC, UPV/EHU) - Materials Physics Center MPC, Paseo Manuel de Lardizabal 5, E-20018 San Sebastián, Spain
l IKERBASQUE - Basque Foundation for Science, Plaza Euskadi 5, E-48009 Bilbao, Spain

ARTICLE INFO

ABSTRACT

Cellular membranes are complex systems that consist of hundreds of different lipid species. Their investigation often relies on simple bilayer models including few synthetic lipid species. Glycerophospholipids (GPLs) extracted from cells are a valuable resource to produce advanced models of biological membranes. Here, we present the optimisation of a method previously reported by our team for the extraction and purification of various GPL mixtures from *Pichia pastoris*. The implementation of an additional purification step by High Performance Liquid Chromatography-Evaporative Light Scattering Detector (HPLC-ELSD) enabled for a better separation of the GPL mixtures from the neutral lipid fraction that includes sterols, and also allowed for the GPLs to be purified according to their different polar headgroups. Pure GPL mixtures at significantly high yields were produced through this approach. For this study, we utilised phoshatidylcholine (PC), phosphatidylserine (PS) and phosphatidylglycerol (PG) mixtures. These exhibit a single composition of the polar head, *i.e.*, PC, PS or PG, but contain several molecular species consisting of acyl chains of varying length and unsaturation, which were determined by Gas Chromatography (GC). The lipid mixtures were produced both in their hydrogenous (H) and deuterated (D) versions and were used to form lipid bilayers both on solid substrates and as vesicles in solution. The supported lipid bilayers were characterised by quartz crystal microbalance with dissipation monitoring (QCM-D) and neutron reflectometry (NR), whereas the vesicles by small angle X-ray (SAXS) and neutron scattering (SANS). Our results show that despite differences in the acyl chain composition, the hydrogenous and deuterated extracts produced bilayers with very comparable structures, which makes them valuable to design experiments involving selective deuteration with techniques such as NMR, neutron scattering or infrared spectroscopy.

1. Introduction

Cellular membranes act as natural barriers in separating the extracellular environment from the array of discrete cellular organelles. They also provide the interfaces wherein chemical reactions and other biological processes occur. Glycerophospholipids (GPLs), glycolipids, sphingolipids and sterols are the main components of cellular membranes [1,2]. In particular, GPLs are the most abundant and not only act as key architectural components of the membrane, but also partake in a host of biological functions. Typically, a GPL molecule consists of two hydrophobic acyl chains coupled to the polar head-bound phosphate through a glycerol backbone. Classification of GPLs is based on the chemical nature of the polar head; with it being zwitterionic in the case of phosphatidylcholine (PC) and phosphatidylethanolamine (PE), whereas it is anionic in phosphatidylserine (PS), phosphatidylinositol (PI) and phosphatidylglycerol (PG). Further, each of these classes comprises a multitude of molecular species through variations in the hydrocarbon chain length as well as in their extent of unsaturation. The possibility of having all such combinations has led to the existence of thousands of structurally distinct GPLs, each potentially contributing to the properties of cellular membranes and the biological processes occurring within them [3].

Because of the high level of compositional complexity of cellular membranes, their biophysical investigation often reduces to the use of simple model systems composed of only one to three synthetic GPL species [4–7]. While such membrane models have been insightful in helping to understand the fundamental aspects of membrane structure and function, they are far from real biological systems. On the other hand, developing biochemical protocols for the extraction of GPLs from natural membranes enables the production of more complex lipid membranes, which can be used to establish a closer link between the model and native systems [5]. Specifically, eukaryotic or bacterial cells can be used to extract physiologically relevant GPL mixtures containing numerous unsaturations in their acyl chains, which, at present, are impossible to be chemically synthesized with existing strategies, especially in the deuterated form [8–10]. Nevertheless, the main challenges in the production of GPL mixtures from natural sources concern their isolation from other chemical species, the experimental reproducibility, the detailed characterisation of the chemical composition of the extracts, and the final amounts that are often in the microgram scale while for many structural characterisation studies milligrams are needed.

Here we report an optimised experimental protocol for the isolation and purification of GPLs from the yeast *Picha Pastoris*. We demonstrate that such GPLs are suitable for the production of more advanced membrane models compared to state-of-the art systems including synthetic lipids. The produced lipids were characterised with biophysical methods both in solution and deposited onto solid substrates. Furthermore, we discuss the production and characterisation of the same membrane models with deuterated GPLs obtained from *P. pastoris* cells grown in a deuterated culture media. Such deuterated membrane models are crucial for enhancing the amount of information that can be obtained with techniques such as NMR, IR and neutron scattering, and are therefore relevant for a broad range of scientific cases [11–14]. In addition, a membrane system composed of adequately deuterated natural GPL mixtures can act as a single invisible support for protein or peptide studies, thus helping understand molecular interplays within such membranes. Currently existing deuteration approaches consist of expensive synthetic routes, primarily with the ability of producing only fully saturated or mono-unsaturated molecules [15]. In contrast, 'biological deuteration' is based on enzymatically-synthesised perdeuterated GPLs, which can be extracted from living cells, and hence represent a more promising approach for the production of perdeuterated lipids at large scales. [16–19]. Recently, it has been shown that the methylotrophic yeast *P. pastoris* can be adapted to grow in D_2O supplemented media, therefore being a valuable source for deuterated GPL species [17]. Although *P. pastoris* has been widely used for heterologous protein expression,

it has not been extensively employed as a cellular factory for producing lipids, in spite of its ability to synthetise the full range of biological lipids representative of the mammalian phospholipidome [20].

Our team pioneered the characterisation of lipid membranes prepared with hydrogenous and deuterated lipids extracted from *P. pastoris* both in solution (vesicles) or in the proximity of a solid substrate (supported lipid bilayers, SLBs) [21–27]. In these previous studies, we mainly used the total lipid extract and the total GPL extract, which include different lipid species, in the first case, and different phospholipid classes, in the second case. We therefore relied on the natural abundance of the different lipid and GPL species within the *P.pastoris* cellular membranes. However, controlling the membrane composition is a desirable aspect in the design of membrane models as it allows to tune the membrane lipid composition depending on the kind of membrane to be mimicked. We also reported that the GPL biosynthetic processes in *P. pastoris* and *E. coli* are significantly affected upon deuteration resulting in alterations in the molecular compositions of the lipid extracts [17,22], although the underlying mechanism behind this phenomenon has not been well understood.

In this study, we describe an optimised purification method which allows to better separate the GPL mixtures from the other lipid classes and obtain better yields when compared to the approach previously employed [17]. Briefly, the introduction of an additional purification step consisting of an HPLC-ELSD coupled to a normal phase silica column setup enables for a better separation of the GPL mixtures from other neutral lipids, such as sterols, as well as to differentiate them according to the different head groups. Such an approach allowed us to produce natural GPL mixtures that were very pure at significantly high yields as compared to what has been achieved previously [22,21]. More specifically, from the *P. pastoris* GPL extract: PC, PS and PG mixtures were produced both in their hydrogenous (hPC, hPS, hPG) and deuterated (dPC, dPS, dPG) forms. Each of these mixtures consisted of a single polar head species bound to different kinds of acyl chains, of which the chemical composition and relative abundance were determined. In this study, hPC and dPC membranes were used as a reference, and PC, PS and PG lipid mixtures were combined to produce dPC/dPS, hPC/hPS and dPC/dPG, hPC/hPG bilayers with 20% w/w of either PS or PG. Such PC/PS and PC/PG mixtures are particularly relevant membrane models as they enable tuneable content of negatively charged lipids while having a biologically relevant composition of the acyl chains. The produced lipid mixtures were used to form membranes in the form of vesicles, SLBs and lipid monolayers, which were structurally investigated with solution scattering techniques, *i.e.*, small angle X-ray and neutron scattering, and surface sensitive techniques, *i.e.*, quartz crystal microbalance with dissipation monitoring (QCM-D) and neutron reflectometry (NR). In contrast to previous studies [22,24,21], here we suggest that the higher purity of the produced GPL extracts enables the formation of hydrogenous and deuterated SLBs by vesicle fusion at room temperature.

Altogether, we show how natural GPL mixtures extracted from *P. pastoris* can be purified according to the different polar headgroups and used to produce advanced models of biological membranes both in their hydrogenous and deuterated forms. These model membranes show great promises towards a better understanding of the structure and function of biological membranes as well as their mechanisms of interaction with biomolecules like proteins and peptides, or drugs.

2. Materials and methods

2.1. Chemicals and reagents

Hydrogenous and deuterated extracts (H or D-total extracts) were obtained from *P. pastoris* yeast cells grown in H_2O or D_2O media as described below. Synthetic GPL standards [POPC, POPS, POPI, POPE and POPG where PO corresponds to 1-palmitoyl-2-oléoyl-sn-glycéro] (≥ 99% purity) were purchased from Avanti Polar Lipids, Inc. (Alabaster, AL) and used as supplied. Heavy water (D_2O 99.9% purity) and

all the HPLC-grade solvents including $CHCl_3$ ($\geq$ 99.5% purity), C_2H_5OH (98% purity), C_3H_6O (98% purity), C_6H_{14} (98% purity) and CH_3OH (99.8% purity), were purchased from Sigma-Aldrich and used without any further purification. d8-Glycerol was obtained from Euriso-Top, France. Stationary phase silica columns for solid phase extraction and a semi-preparative Nucleosil 100-5 OH column were purchased from Macherey-Nagel, France. All other chemicals and cell culture media components were obtained (in the highest commercially available purity) from Sigma Aldrich, France.

2.2. Natural GPL mixtures preparation

2.2.1. Cultivation of P. pastoris

P. pastoris GS115 HSA (*Invitrogen*) cells were cultured in the deuteration facility of the Institut Laue-Langevin (D-Lab, ILL), Grenoble, France, using the protocol described earlier [17]. In brief, cells were grown at 30 °C in 10 mL of BMGY medium (10 g/L yeast extract, 20 g/L peptone, 5.96 g/L KH_2PO_4, 1.07 g/L K_2HPO_4, 13.4 g/L yeast nitrogen base with ammonium sulphate without amino acids, 4 mg/L biotin, 10 g/L glycerol) in a 100 mL Erlenmeyer flask (Corning) using vent caps for continuous gas exchange with shaking at 250 rpm. After 4 days, 1 mL of this pre-culture was diluted into 100 mL of minimal medium (38.1 g/L H_3PO_4, 0.93 g/L $MgSO_4$, 4.13 g/L KOH, 20 g/L glycerol, 0.4 mg/L biotin, 40 mg/L histidine, 26 mg/L cupric sulphate pentahydrate, 0.35 mg/L sodium iodide, 13 mg/L manganese sulphate monohydrate, 0.87 mg/L sodium molybdate dehydrate, 0.09 mg/L boric acid, 2.17 mg/L cobalt chloride, 87 mg/L zinc chloride, 0.28 g/L ferrous sulphate heptahydrate, 87 mg/L biotin, 40 mg/L sulphuric acid; the pH was adjusted to 6.0 using NH_4OH) and incubated at 30 °C for 2-3 days with shaking at 250 rpm. For the adaptation of perdeuterated *P. pastoris*, 1 mL of the culture in minimum medium was diluted into 100 mL of perdeuterated basal salt medium (d-BSM) and incubated at 30 °C for 5–6 days. The deuterated medium was prepared as follows: 1 L of hydrogenated basal salt medium (h-BSM) without glycerol was flash evaporated, the powder re-suspended in 250 mL of 99.85% D_2O (Eurisotop) and flash evaporated again. This process was repeated twice to get rid of H_2O traces. Finally, the powder was re-suspended in 1 L D_2O (purity >99.9%, Euriso-top) containing 20 g d8-glycerol (Euriso-top). The deuterated culture was diluted again in D-minimal medium and grown for 2–3 days and used as inoculum for the final deuterated culture. 1 mL of each H- or D-pre-culture was taken to inoculate 150 mL of h-BSM and d-BSM and incubated at 30 °C. The initial optical cell density (OD_{600}) was approximately 0.3 for all the cultures. Cells upon entering the exponential phase were harvested by centrifugation and frozen at -80 °C.

2.2.2. Total lipid extraction

GPL mixtures were extracted and purified from perdeuterated and hydrogenous *P. pastoris* biomasses. Harvested cells were suspended into 10 mL Milli-Q H_2O (18 MΩ cm at 25 °C, Millipore) and lysed by tip-sonication (Bandelin SONOLPULS HD 3100 ultrasonic homogenizer) on an ice bath for 3×5 min with 30 s intervals, 20% duty cycle. The cell lysate was poured into boiling C_2H_5OH (at 95 °C) containing 1% butylated hydroxytoluene (BHT) followed by vigorous stirring in order to denature lipases. The total lipid mixtures were then extracted according to the method of Bligh and Dyer [28], followed by evaporation of the organic phase using a rotovapor and their final reconstitution in C_6H_{14}.

2.2.3. Separation of GPL mixtures by preparative HPLC

Separation of the various classes of GPL mixtures was achieved through sequential purification steps: first by passing the sample through an amino-bonded solid-phase extraction (SPE) column; followed by the evaporation of the eluate fractions (containing the polar lipid mixtures) using a rotovapor and their subsequent reconstitution in $CHCl_3/CH_3OH$ [95:5]. The polar fraction was next injected through

a diol-modified silica stationary phase column (semi-preparative Nucleosil 100-5 OH column [10 x 250 mm] (Macherey-Nagel, France)) coupled to an Agilent chromatographic system (1260 Infinity II series, Agilent Technologies, France), with SEDEX 90 ELSD as a detector (Sedex Sedere, France).

An HPLC-gradient was performed in order to elute the GPLs. The gradient method utilised solvent mixture A [$CHCl_3$ - CH_3OH] (70:25 v/v) containing 1% NH_4OH and solvent mixture B [$CHCl_3$ - CH_3OH - H_2O] (60:40:5.5 v/v/v) that contained 0.5% NH_4OH that was run at a flow rate of 1.0 mL/min. A method was programmed such that at time zero, the proportion of solvent mixture B was 5% and gradually increased to 40% at 40 min, then to 100% at 60 min and stayed at this value until 95 min after which it was again decreased to 5% at 96 min and kept there until the end of the gradient at 105 min. During all the measurements, the column temperature was maintained at room temperature, whereas the ELSD temperature was set at 60 °C where N_2 was used as a carrier gas at 3.5 bars inlet pressure. Data were analysed by the Open Lab chromatographic workstation (Agilent Technologies, France).

2.3. Molecular compositional analysis of the purified GPL mixtures

2.3.1. GPL mixture analysis by High-Performance Thin Layer Chromatography (HPTLC)

In order to assess the identity and purity of each of the purified classes, 5.0 - 10.0 μ g of the fractionated samples (evaporated under Argon (Ar) and reconstituted in 1 mL of $CHCl_3/CH_3OH$ [2:1]) and standards were applied to a silica gel 60 (F_{254}) pre-coated TLC plate of 0.2 mm layer thickness, with a CAMAG LINOMAT5 sample applicator (CAMAG, Mutten, Switzerland) fitted to a 100 μ L micro-syringe. Samples were applied at a constant application velocity of 150 nL/s under a continuous stream of N_2 gas. The TLC plate was next preconditioned and then developed in a CAMAG twin-trough-chamber filled-in with a mobile phase, [$CHCl_3$-CH_3OH-CH_3COOH] (65:28:8 v/v/v). Finally, the developed plate was derivatised using a 1.5% $CuSO_4$ solution sprayed over it in the CAMAG derivatiser chamber following which, it was dried on a hot plate at 120 °C for 10 min for the development of spots. Further, the developed spots were visualized and analyzed in a CAMAG TLC scanner 3 using the winsCATS software (*version* 1.4.6).

2.4. FAMEs analysis by Gas Chromatography (GC)

Global acyl chain composition of both the hydrogenous and deuterated total lipid extracts from *P. pastoris* were initially determined by Gas Chromatography-Mass Spectrometry (GC-MS), [Agilent, 5977A-7890B] and that of the purified mixtures were carried out by Gas Chromatography-Flame Ionization Detection (GC-FID), [GC 2010 Plus, Shimadzu], after methanolysis to release the fatty acids as their corresponding fatty acid methyl esters (FAMEs). The total fatty acid analyses by GC-MS were carried out by first drying 50 μL of the samples using a vacuum pump and then derivatised using trimethyl sulfonium hydroxide (TMSH) (Machery-Nagel) to obtain the corresponding FAMEs. The samples were next injected into a GC-MS, according to the method described by [29] and [30] followed by their identification based on their retention times and mass spectra compared to authentic fatty acid standards (Sigma). FAMEs were identified from their mass spectra and retention times and quantified by Mass Hunter Quantification Software (Agilent) and normalised by PC-21:0/21:0 as an internal standard. The mass spectra of each fatty acid species were obtained from its peak in the total ion chromatogram (TIC) and compared between the hydrogenous and deuterated lipid extracts.

In order to run GC-FID measurements, the samples were derivatised upon adding about 3 mL of methanolic-HCl to glass vials containing 0.1 mg to 1 mg of the lipids extracts. The vial tubes were then bubbled with Ar, vortexed and sealed tightly with a Teflon-lined cap and

incubated at 85 °C for 1 h. After cooling down the vials to room temperature ($\approx$ 10 min), 3 mL of H_2O were added and the solution vortexed, following which 3 mL of C_6H_{14} were added and again vortexed vigorously to create an emulsion. Slow centrifugation ($\approx$ 500 g for 5 min) at room temperature was carried out to break the emulsion and produce an upper C_6H_{14}-rich phase containing FAMEs. The supernatant phase of $\approx$ 2.8 mL was then transferred into a fresh vial, evaporated under a stream of N_2 and the resulting dried film was reconstituted in 250 μ L C_6H_{14} and transferred into a GC auto sampler vial that was then loaded into the GC's automatic liquid sampler. The GC instrument (GC 2010 Plus, Shimadzu) was equipped with a split/splitless injector and a SGE BPX70 70% Cyanopropyl Polysilphenylene-siloxane column (25 m by 0.22 mm ID and 0.25 μm film thickness). Helium (He) was used as a carrier gas at a flow rate of 1.04 mL/min with a linear velocity of 35 cm/sec and a purge flow rate of 1 mL/min. The column was allowed to equilibrate for 3 minutes at 155 °C before injection and then the temperature was ramped up to 180 °C at a rate of 2 °C/minute and then to 220 °C at a rate of 4 °C/minute and finally held at 220 °C for 5 minutes resulting in a 27.5-minute total run time. Samples (5 μL) were injected into the column at 250 °C using an AOC-20i auto injector. Detection was done using an FID operating at 260 °C with 40 mL/min H_2, 400 mL/min compressed air and 30 mL/min He make-up flow. Data analyses of the FAMEs obtained from the purified GPL mixtures were carried out by LabSolutions software (Shimadzu), which was used to assign and integrate the total ion chromatogram peaks from which the total mole fraction amount of each of the FAMEs were obtained.

2.5. Sample preparation

2.5.1. Vesicle preparation for SANS/SAXS and NR

Large unilamellar vesicles (LUVs) were produced by rehydration of a GPL film in a glass vial. The film was produced by first dissolving natural GPL mixtures in $CHCl_3$, and subsequently drying the desired amount of lipids under a gentle Ar flow. The film was then stored in vacuum overnight to ensure a complete evaporation of the solvent. The film was rehydrated at room temperature in degassed H_2O (or salt solution for the samples used for NR experiments, *see next paragraph*) with a final lipid concentration of 1 mg·mL^{-1}. The vials containing the lipid solution were filled up with Ar to limit the presence of O_2 and then vortexed to fully suspend the lipid film. Immediately before use for supported lipid bilayer (SLB) formation, the suspension was tip-sonicated (Bandelin SONOLPULS HD 3100 ultrasonic homogenizer) for 5 min at pulses of 1-second ON and 6-seconds OFF, 20% amplitude on ice, to produce a visually clear solution of LUVs. For SANS/SAXS measurements, each solution was extruded at room temperature using an Avanti mini-extruder for at least 31 times across a 100 nm pore membrane, in order to favour the formation of monodisperse LUVs. The samples were measured with DLS to confirm the absence of large multilamellar aggregates.

2.5.2. Vesicle fusion protocol - for NR and QCM-D

The LUV suspension used to produce the SLBs were prepared by dissolving the GPL composed film with a 0.5 M NaCl solution, thereafter following the protocol as described above. Immediately after sonication, the LUV suspension (with a final volume of 1.5 mL at 1 mg·mL^{-1}) was injected into the NR/QCM-D cells. About 1.5 mL of solution was sufficient to fill entirely one NR cell and 4 QCM-D cells. Upon equilibration of the LUV suspension in the NR/QCM-D cell (*approx.* 20 min), the cells were rinsed with Milli-Q H_2O. An osmotic shock produced by replacing the salt solution with Milli-Q H_2O favours the fusion of the vesicles at the solid support surface and the formation of an SLB.

2.6. Physico-chemical characterisation

2.6.1. QCM-D

QCM-D measurements were performed with a E4 instrument (Q-Sense, Biolin Scientific AB, Sweden), using SiO_2-coated 5 MHz quartz sensors in the PSCM labs at the ILL. Crystals were cleaned using $CHCl_3$, C_3H_6O, C_2H_5OH and Milli-Q H_2O (18 MΩ cm at 25 °C, Millipore) in a bath sonicator for 15 minutes per solvent. Immediately before use, the crystals were treated with a UV ozone cleaner (BioForce Nanosciences, Inc., Ames, IA) for 30 min. The fundamental frequency and six higher overtones (3rd, 5th, 7th, 9th, 11th and 13th) were recorded in Milli-Q H_2O until a stable baseline was obtained. After exchange with 0.5 M NaCl solution, the samples were injected in the flow cell at 0.1 mL/min, following the vesicle fusion protocol described above. The real-time shifts in the resonance frequency (ΔF_n) with respect to the calibration value (bare crystal in Milli-Q H_2O) were measured for different overtones indicated as F_n, with n representing the overtone number. Simultaneously, also the energy dissipation factor (D) was monitored for all the measured overtones.

2.6.2. SANS

SANS measurements were carried out on the instrument D22 (https://www.ill.eu/users/instruments/instruments-list/d22/description/instrument-layout) at the ILL, using Hellma quartz 120-QS cells of 1 mm pathway. Samples were measured over a q-range of $2.5 \cdot 10^{-3}$–0.6 Å^{-1} at a single wavelength of 6.0 Å (FWHM 10%) with 3 sample-to-detector distances of 1.5 m, 5.6 m and 17.6 m. Absolute scale was obtained from the flux using the attenuated direct beam. Data correction was performed using the software GRASP: (https://www.ill.eu/users/support-labs-infrastructure/software-scientific-tools/grasp), accounting for transmission, flat field, detector noise (measurement of boron carbide absorber); the contribution from the solvent was subtracted.

2.6.3. Neutron Reflectometry (NR)

NR experiments on Langmuir monolayers at the air/liquid interface and on SLBs at the solid/liquid interface were performed on FIGARO [31], a time-of-flight reflectometer at the ILL. Two different angles of incidence, *i.e.* $\Theta_1 = 0.6°$ and $\Theta_2 = 3.7°$ for the air/liquid setup, and $\Theta_1 = 0.8°$ and $\Theta_2 = 3.2°$ for the solid/liquid setup, were used in order to cover a momentum transfer (q_z) range from about $3 \cdot 10^{-3}$ Å^{-1} to 0.25 Å^{-1} in combination with a wavelength range of 2-20 Å for both setups and wavelength resolution of 7% $d\lambda/\lambda$. The momentum transfer q_z is defined as shown in equation (1).

$$q_z = \frac{4\pi}{\lambda} \cdot \sin\theta \tag{1}$$

where λ is the wavelength of the neutron beam. Slits were set in order to have the same surface (under)illumination for the two used angles.

The reflectivity R(q_z), which is defined as the ratio of the reflected intensity over the incident beam intensity (direct beam), was calculated using the software COSMOS [32]. Briefly, the background was measured on the left and right side of the reflectivity signal and directly subtracted from it. The reflected intensity was divided by the direct beam intensity measured using the same slit configuration and overall settings as in reflectivity, but in transmission mode through the incoming media (air or silicon). Measurements on the SLBs at the solid/liquid interface were performed using silicon (111) single crystals as solid substrate (8×5 cm^2 surface and 2 cm thickness), polished on one face (≤ 5 Å roughness). The substrates were cleaned by 15 min ultrasound sonication in the following solvents: $CHCl_3$, C_3H_6O and C_2H_5OH, and at the end Milli-Q H_2O. Subsequently, the substrates were dried using N_2 and treated for 2 min with air plasma cleaner in order to make their surface hydrophilic and remove any remaining trace of organic molecules. Finally, the cleaned substrates were rinsed with Milli-Q H_2O, and assembled into solid/liquid cells. Each of the investigated SLBs was measured in 3 or 4 different contrasts, composed by mixtures of D_2O and H_2O at different ratios: 100% D_2O, 4MW (*Four Matched Water* 66:34 D_2O:H_2O v/v), SMW (*Silicon Matched Water* 38:62 D_2O:H_2O) and 100% H_2O. The scattering length density (SLD) (ρ) of the SMW equals that of the silicon crystal ($\rho = 2.07 \cdot 10^{-6}$ Å^{-2}), while ρ for the 4MW is $\rho = 4.00 \cdot 10^{-6}$ Å^{-2}. For the monolayer measurements, NR experiments

were performed using two mixtures as subphase: 100% D_2O and 8:92 v/v of D_2O:H_2O, known as ACMW (*air contrast matched water*) since its SLD is equal to that of air, *i.e.*, zero.

NR data analysis. The analysis of the reflectivity data was done using a home-developed code, CoruxFit. The samples, were modelled as a series of layers (from now on named "components"), with different chemical composition stacked along the direction normal to the support surface (z) and corresponding, in our case, to different portions of the lipid molecules, *i.e.*, lipid polar head and acyl chains. The following components were used to describe the SLBs under examination: (1) bulk silicon, (2) silicon oxide, (3) inner polar head, (4) hydrophobic chains, (5) outer polar head; and for the monolayer model: (1) polar head, (2) hydrophobic chains, (3) air. A component volume fraction distribution ($\psi(z)$) was assigned to each of the identified components (see the equation (2)).

$$\psi(z) = \frac{1}{2} \cdot \left(erf \frac{z - z_\mu + \frac{d}{2}}{\sqrt{2}\sigma} - erf \frac{z - z_\mu - \frac{d}{2}}{\sqrt{2}\sigma} \right) \cdot (1 - \phi_{solv}) \quad (2)$$

where *erf* is defined as follows:

$$erf(x) = \frac{2}{\sqrt{\pi}} \int_0^x e^{-t^2} dt \quad (3)$$

In equation (2), z_μ describes the position of the component along z; d describes its thickness and σ is the roughness of the interface between two consecutive components. Each component is scaled by its amount of water, through the parameter ϕ_{solv}. Next, the water profile is calculated, adding up to 1 every component, if the component itself does not reach 1 (see equation (4)).

$$\Psi_{solv}(z) = 1 - \sum_{i=1}^{n_{comps}} \psi_i(z) \quad (4)$$

where $\Psi_{solv}(z)$ is the total fraction of water along z and n_{comps} is the total number of components of the model. The thicknesses associated to each lipid component are calculated using the lipid volumes and the topological area per lipid (A_{lipid}). Mono-unsaturated lipids are expected to have a cylindrical shape. Although the characterisation of the lipid mixture composition showed also the presence of lipids with 2-3 unsaturations, which imply a non-cylindrical shape, because of the largest abundance of the mono-unsaturated lipids, in the used model the polar head (PH) and the acyl chains (CH) are constrained to have the same area per lipid (equation (5)).

$$t_{PH} = \frac{PH_{vol}}{A_{lipid} \cdot (1 - \phi_{PH_{hydr}})} \quad \text{and} \quad t_{CH} = \frac{CH_{vol}}{A_{lipid}} \quad (5)$$

t_{PH} and t_{CH} are the thicknesses of the layers for the polar head and chains respectively, V_{PH} and V_{CH} are the polar head and acyl chain region volumes, the A_{lipid} is the topological area per lipid and $\phi_{PH_{Hydr}}$ is the hydration water of the polar head. The average molecular volumes of the hydrophobic tails were calculated using the data provided by the GC-FID analysis (see Fig. 2), and by considering the following volumes for lipids in the fluid phase (22 °C and 37 °C): $Vol_{CH_2} = 27.5$ Å^3, $Vol_{CH_3} = 55.1$ Å^3, $Vol_{CH} = 22.2$ Å^3 [33]. The volumes for the different polar heads were calculated from the relative mass density (PC-$V_{PH} = 318$ Å^3, PS-$V_{PH} = 263$ Å^3, PG-$V_{PH} = 288$ Å^3). The V_{PH} are left varying in a small range during the fit. The polar head and acyl chain SLDs for the hydrogenous lipids were calculated summing all the scattering lenghts of each atom in the polar head or acyl chain region and by dividing up for their corresponding volumes. For the deuterated lipids, the SLDs were fitted, since such natural mixtures are not exactly 100% deuterated. From these fits, we were able to calculate the percentage of deuteration for each lipid class (PC, PS and PG). In summary, the fitted parameters are the following: (1) A_{lipid}; (2) ϕ_{CH}; (3) $\phi_{PH_{Hydr}}$; (4) σ

and (5) ϕ_{ox}; where the parameter (2) corresponds to the amount of water through the bilayer (defects in the bilayer) and the complement to 1 of ϕ_{CH} (1 - ϕ_{CH}) is the coverage of the bilayer on the surface of the silicon crystal; (3) is the amount of hydration water in the polar head region, whereas ϕ_{PH} (amount of water in polar head region including the water fraction related to the presence of defects in the bilayer, which corresponds to ϕ_{CH}, as no water is expected among the acyl chains unless the bilayer is not fully covering the supporting surface) calculated as: $\phi_{PH_{Hydr}} + \phi_{CH}$; (4) is the interface roughness and (5) is the amount of water in the oxide layer of the silicon crystal. In addition, the SLD of the solvent was fitted to the experimental data with a fixed range corresponding to ±10% the expected value based on the solvent nominal composition (i.e. % v/v of D_2O in the mixture).

For the bilayer measurements, the parameters describing the oxide layer were previously fitted using the data collected on the bare surfaces in two contrasts, and were kept constant during the fit of the bilayer parameters (except the ϕ_{ox}, that can be different between bare and occupied surfaces). This approach decreases the number of fitted parameters and leads to an improvement in the accuracy of the final result.

The total SLD profile is calculated by multiplying each error function of the final model for the corresponding SLD value, and by summing them all together to have the complete SLD profile. The theoretical reflectivity curve is calculated using the Parrat algorithm [34], with the SLAB method.

The minimization routine has two algorithms in series based on the chi square minimisation; the first one is the simulated annealing, useful to test the whole parameter range avoiding relative minimums; once the best solution is found, the second algorithm is used, based on the steepest descent (link to the python library: https://docs.scipy.org/doc/scipy/reference/generated/scipy.optimize. least_squares.html), that cools down the system, and finds the best parameter combination with the lowest chi square. Errors for the fitted parameters were calculated as the square root of the diagonal elements in the inverse Hessian matrix. From the non-diagonal element of this matrix it is also possible to obtain the correlation (positive, negative or neutral) between the fitted parameters. These are useful to assess the accuracy of the used model. The errors for the derived parameters, such as the bilayer thicknesses, are calculated with the standard error propagation. The q resolution of the instrument is also taken into account during the calculation of the theoretical reflectivity profiles.

2.6.4. Small Angle X-ray Scattering (SAXS)

SAXS experiments were performed on the beamline BM29, ESRF, Grenoble, France (Pernot et al. [35]), using a Pilatus3 2M detector at a sample-detector distance of 2.867 m. 20 frames each for 2 s were recorded at 22 °C, a sample concentration of 2 mg·mL^{-1} in a 1 mm flow-through quartz capillary and a photon energy of 15 keV. Data reduction and normalisation were done by the automated ExiSAXS user interface. Solvent and capillary contributions were subtracted by using SAXSutilities 2 (www.saxsutilities.eu accessed on 21 October 2021).

SAXS data analysis. SAXS data were analysed using a simple smeared 3-slab model [36], the slabs representing lipid polar heads (PH), acyl chains (CH) and the terminal methyl groups (T). Error-functions of widths d_k ($k \in \{PH, CH, T\}$) and standard deviations σ_k were used to mathematically describe the slabs. Additionally, we included an acyl chain thickness polydispersity by averaging over a Gaussian distribution $\mathcal{N}$ with mean d_{CH} and standard deviation σ_{poly} (see also [37]). The model does not include specific lipid compositions and therefore all scattering length densities ρ_k are provided in arbitrary units. $\Delta\rho_k = \rho_k - \rho_0$ designates the contrast to the H_2O-background. The vesicle form factor is approximated by the Lorentz-factor q^{-2}. The full model for the scattering intensity I(q), including a uniform background I_0 is given by:

Table 1
Yields of each purified class of GPL molecules, starting from 5 g of *Pichia pastoris* cell paste.

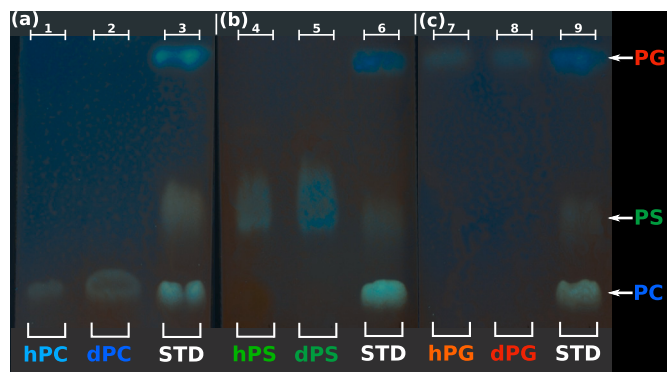| GPL class	Hydrogenous [mg]	Deuterated [mg]
PC	65	69
PS	32	20
PG	17	11

Fig. 1. TLC analysis of the HPLC-purified GPL mixtures from *P.pastoris*. Image (a) shows the purified 'H' [Lane 1] and 'D' [Lane 2] PC mixtures and [Lane 3] corresponds to the standard mixture containing a single molecular species each that of PC, PS and PG. [Lane 4 and 5] in image (b) show the purified 'H' and 'D'-PS mixtures and their corresponding ladder in [Lane6]. Similarly, [Lane 7 and 8] in image (c) correspond to the purified 'H' and 'D'-PG mixtures respectively and the marker lane in [Lane 9].

$$
\begin{aligned}
I(q) \propto 2q^{-4} \sum_i &\mathcal{N}(d_{CH,i} \vee \overline{d}_{CH}, \sigma_{poly}) \mid 2\Delta\rho_{PH}e^{-\sigma_{PH}^2 q^2} sin(qd_{PH}/2) \\
&\times cos[q(d_{CH,i} + d_{PH}/2)] \\
&+ 2\Delta\rho_{CH}e^{-\sigma_{CH}^2 q^2} sin(qd_{CH,i}/2)cos[q(d_T + d_{CH,i}/2)] \\
&+ \Delta\rho_T e^{-\sigma_T^2 q^2} sin(qd_T/2) \mid^2 + I_0
\end{aligned}
\tag{6}
$$

The model was constrained by the assumptions $\sigma_{PH} = \sigma_{CH}$ and $\sigma_T = 2.5$ Å. Parameter optimization was by a Trust Region Reflective algorithm from the SciPy 1.6.2 package [38].

3. Results

3.1. Purification and composition of the deuterated and hydrogenous GPL mixtures

Compared to previous preparations of *P. pastoris*-GPL mixtures reported by our team [22,21], an additional improvised purification step by HPLC-ELSD was included in the sample preparation protocol (see *Materials and Methods* and *Supplementary Materials* paragraph S1.1). This additional purification step, enabled us to increase the purity of the GPL mixtures, as well as to separate them according to their different classes, e.g. PC, PS and PG, at significantly high yields as listed in Table 1. It also allowed us to observe that the deuterated extract exhibited a higher content (*approx.* by a factor of 1.7) of neutral lipid (e.g. sterols, steryl esters) compared to their hydrogenous counterpart (see further details in *Supplementary Material* Fig. S1). Separation of the GPL mixtures by HPLC-ELSD was followed by High Performance Thin Layer Chromatography (HPTLC) analysis of the fractions collected to confirm their identity and purity (see Figs. 1a, 1b and 1c).

Once the PC, PS and PG-GPL mixtures were isolated, we determined the composition of their corresponding acyl chains by GC-FID analysis (*Supplementary Material*, Table S1). Fig. 2: shows the relative abundance of the different acyl chain species that are present in both the deuterated and hydrogenous purified GPL mixtures. In all cases, and in agreement with previously reported results [23,24], C18 acyl

chains mono-unsaturated were the most predominant species. Nevertheless, some differences in the relative amount of the different acyl chains emerged between PC, PS and PG mixtures. As an example, the content of C16:0 is much larger in the PS mixture compared to PC and PG. This suggests that the acyl chain composition exhibits some level of specificity depending on the polar head. Also in agreement with our previous findings [21,22], the composition of the acyl chain was affected by the presence of D_2O in the culture media. The most remarkable effect is the higher concentration of the C18:1 acyl chain compared to the corresponding hydrogenous lipid extract (*as shown in* Fig. 3). This effect is systematically observed in all the investigated GPL classes, although further analysis is needed to deeply understand how D_2O promotes this different abundance of the acyl chains (*as seen from* Fig. 2). The analysis of the acyl chain composition was repeated for all GPL mixtures post preparation of the lipid vesicles (*Supplementary Material*, Fig. S3), which were either used for the formation of the SLBs or directly characterised in solution. No difference in composition was observed, therefore suggesting that the used sample preparation protocol allowed a uniform solubilisation of the lipids (For further details see *Materials and Methods*).

3.2. Physico-chemical characterisation

3.2.1. Phosphatidylcholine (PC) bilayers

Hydrogenous (hPC) and deuterated (dPC) PC bilayers were produced as SLBs, vesicles, and lipid monolayers. A preliminary characterisation of the dPC SLB was performed with QCM-D. The main goal of this initial measurement was to test whether vesicle fusion could be implemented to produce an SLB at room temperature. Fig. 4: shows the collected QCM-D measurements. After calibration of the sensor in Milli-Q H_2O ($\Delta F = 0$) followed by injection of 0.5 M NaCl solution (ΔF approx. -10 Hz), that was used for the vesicle preparation, the dPC vesicle solution was introduced into the cell. Adsorption of the vesicles on the sensor surface is clearly detected by the large decrease of ΔF and parallel increase of ΔD. After approximately 10 min, Milli-Q H_2O was reintroduced into the cell. The osmotic shock induced by the transition from the salt solution to the Milli-Q water favoured the rupture of the initially adsorbed vesicles and the formation of an SLB as indicated by the stable ΔF value of -26 Hz and the dissipation $\Delta D \approx 0$. The SLB signal was monitored over a large time-range and no further variation was observed. Altogether the collected data validate the vesicle fusion method for the production of SLBs with PC lipids. The structural characterisation of the hPC and dPC-SLBs was performed by NR measurements. Fig. 5: shows the NR experimental data together with the corresponding fitting curves for hPC (Panel 5a) and dPC (Panel 5c). Data were analysed as described in the *Materials and Methods* section and by implementing a standard model representing the SLB as a stack of the following components: (i) inner lipid polar heads; (ii) acyl chains; (iii) outer lipid polar heads. Preliminary data analysis showed that the SLB exhibited a symmetric structure with similar structural parameters associated with the inner and outer lipid polar heads. Therefore, in the final data analysis these components were constrained to have the same structure. In order to further reduce the amount of fitted parameters, the area per lipid associated to the polar heads and the acyl chains was constrained to be the same, as expected for PC lipids [39].

NR confirmed the successful formation of an SLB both in the case of hPC and dPC (Fig. 5, Panels b and d). The structure of the two SLBs was very similar, despite the slightly different acyl chain composition of the hPC and dPC lipids (Table 2). The scattering length density associated to the dPC polar heads and acyl chain was optimised to the experimental data in order to extract information on the deuteration level of these lipids. As a result, a deuteration level of 95.4 ± 0.5% for both the polar heads and the acyl chains was estimated. This result was also confirmed by the analysis of the match point performed on dPC vesicles by means of small angle neutron scattering (SANS) measurements (*Supplementary Material* Fig. S4). In such an experiment, dPC vesicles were suspended in
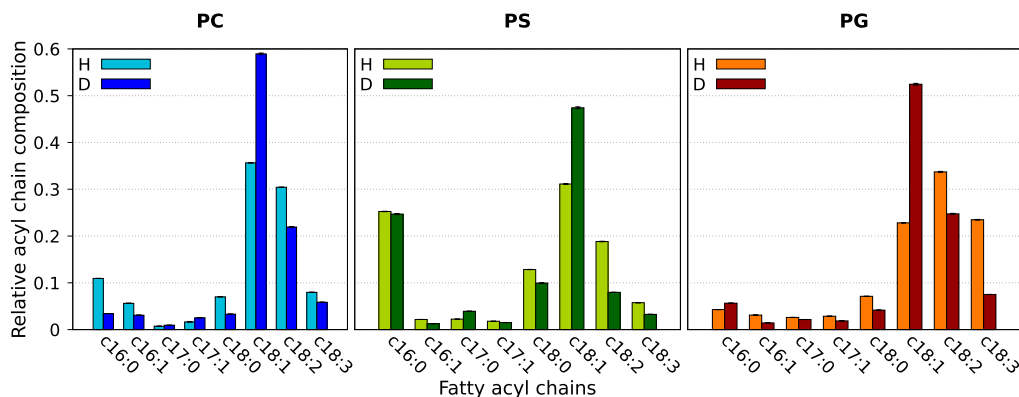
Fig. 2. GC-FID analysis of the fatty acid distribution for the investigated GPL classes. Data are mean ± S.D. of three technical repeats. A complete table with all the values can be found in *Supplementary Material* Table S1.
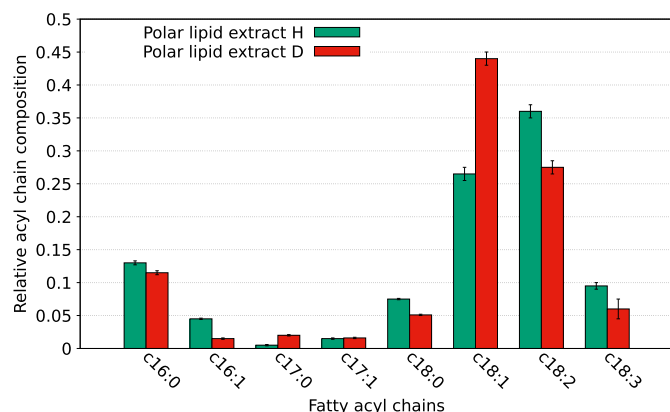

Fig. 3. GC-MS analysis of the fatty acid distribution for the 'H' and 'D' total lipid extracts. Data are mean ± S.D. of three independent experiments.

solutions prepared with increasing D_2O content. The match point corresponds to the D_2O percentage at which the scattered intensity from the vesicles was identical to that of the solvent. The scattering length density of the lipids was calculated from the composition of the solvent at the match point. In case of the dPC lipids, the match point was extrapolated at 109 ± 2% of D_2O (see in *Supplementary Materials* Fig. S4 and Table S2), which corresponds to a deuteration of 97 ± 1%, in good agreement with the NR result.

Vesicles consisting of the PC lipids were also produced for further structural investigation by means of small angle X-ray scattering (SAXS) measurements. The formation of multilamellar vesicles was observed as suggested by the presence of Bragg peaks in the collected data (see *Supplementary Material*, Fig. S5). This is most likely related to the lack of net charges in the lipid polar heads, which favours the stacking of different lamellae. The presence of multilamellar vesicles prevents a good estimation of the bilayer structure and therefore for the PC lipids we rely on the more accurate structural information provided by NR, where multilamellarity was not found in any of the SLB examined.

Finally, lipid monolayers of purely hPC and dPC were also prepared at the air/water interface. Their structure was found to be as shown in *Supplementary Material*, Fig. S6. The structure of the monolayer was characterised by means of NR measurements and resulted in reasonable agreement with the hPC and dPC-SLBs (Table 1 and Table S3).

3.2.2. Phospatidylcholine - Phosphatidylserine (PC/PS) bilayers

Lipid bilayers in the form of SLBs and vesicles in solution were analysed also in the case of the hydrogenous and deuterated mixtures of PC and PS lipids (80/20 w/w). Such mixtures were produced by first

purifying the PC and PS lipids from the total GPL extract from *P. pastoris*, and subsequently recombining them at the desired ratio. Initial formation of the SLB in case of the dPC/dPS mixture was monitored by QCM-D (*Supplementary Material*, Fig. S7). The data showed a similar trend as reported in Fig. 4 and indicated a successful formation of an SLB by vesicle fusion. Structural information on both the hPC/hPS and dPC/dPS bilayers was obtained from the analysis of the NR data (Fig. 6a and 6c). The experimental data were analysed with a similar model compared to the one described above for the PC lipids, but in this case the SLD values were estimated by taking into account the chemical composition of the PC and PS mixtures for acyl chains (Fig. 2) and for the polar head region.

Mixing PS lipids with PC did not produce a significant change in the structure of the SLB compared to the pure PC containing SLB. Both in the case of the hPC/hPS and dPC/dPS SLBs, the bilayer exhibited a high surface coverage, *i.e.*, ≥ 98%. This confirms the vesicle fusion method with the experimental conditions described in the *Materials and Methods* section as suitable for producing high quality SLBs also for lipid mixtures containing negatively charged lipids.

As for the PC-SLB, deuteration of the PS did not significantly affect the bilayer structure, despite the fact that the chemical composition of the acyl chains for both PC and PS was slightly different in the hydrogenous versus deuterated extract. Indeed, both the hPC/hPS and the dPC/dPS bilayers exhibited very similar structural parameters (Table 2). This result was confirmed by the SAXS characterisation of the vesicles prepared from the hPC/hPS and dPC/dPS mixtures (Fig. 6e). The experimental data exhibited the characteristic trend corresponding to unilamellar vesicles and were analysed with a standard bilayer model (see further details in *Materials and Methods* and Table 2). The structure of the bilayer, also represented in the SLD profile (Fig. 6f), is in good agreement with the NR results, and therefore suggests a very similar structural organisation of these lipid mixtures both in solution and in the proximity of a solid substrate.

3.2.3. Phospatidylcholine - Phosphatidylglycerol (PC/PG) bilayers

Alongside with PS, PG is among the most abundant negatively charged lipid in biological membranes [1]. Therefore, binary mixtures of PC and PG lipids are considered simple, but biologically relevant for the production of membrane biomimics. PG lipid mixtures were also purified from the *P. pastoris* GPL extract and produced in their hydrogenous and deuterated version. The same protocol used for the pure PC and the PC/PS mixtures, was used in this case to produce SLBs. Figs. 7a and 7c show the NR experimental data collected for the hPC/hPG and dPC/dPG mixtures respectively. As in the case of the PC/PS mixtures, the content of PG lipids in the mixture was 20% w/w. The collected experimental data were analysed with the bilayer model described above. In addition, the good agreement between the fits and the experimental data suggested the successful formation of an SLB with high sur-
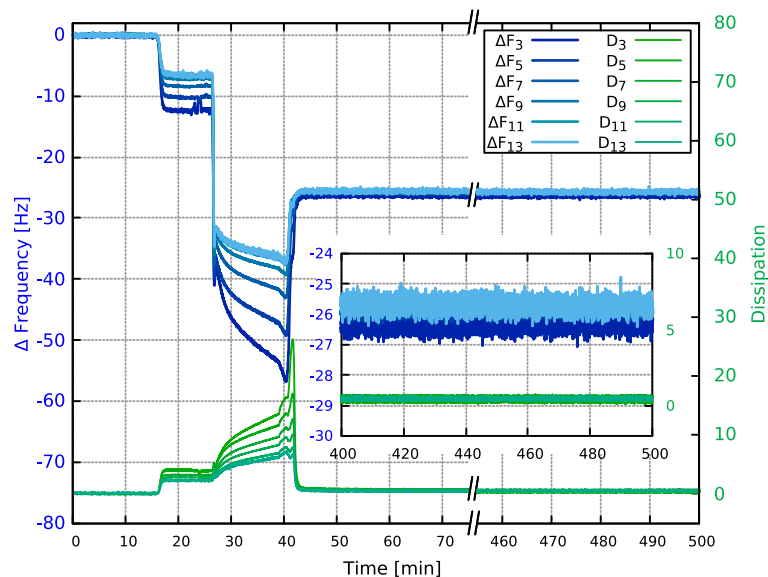
Fig. 4. QCM-D data collected during the formation of the dPC SLB *via* vesicle fusion. The inset shows the region of the curve corresponding to the SLB being formed at the sensor surface. The measurement was performed in parallel in 4 cells, with analogous results.
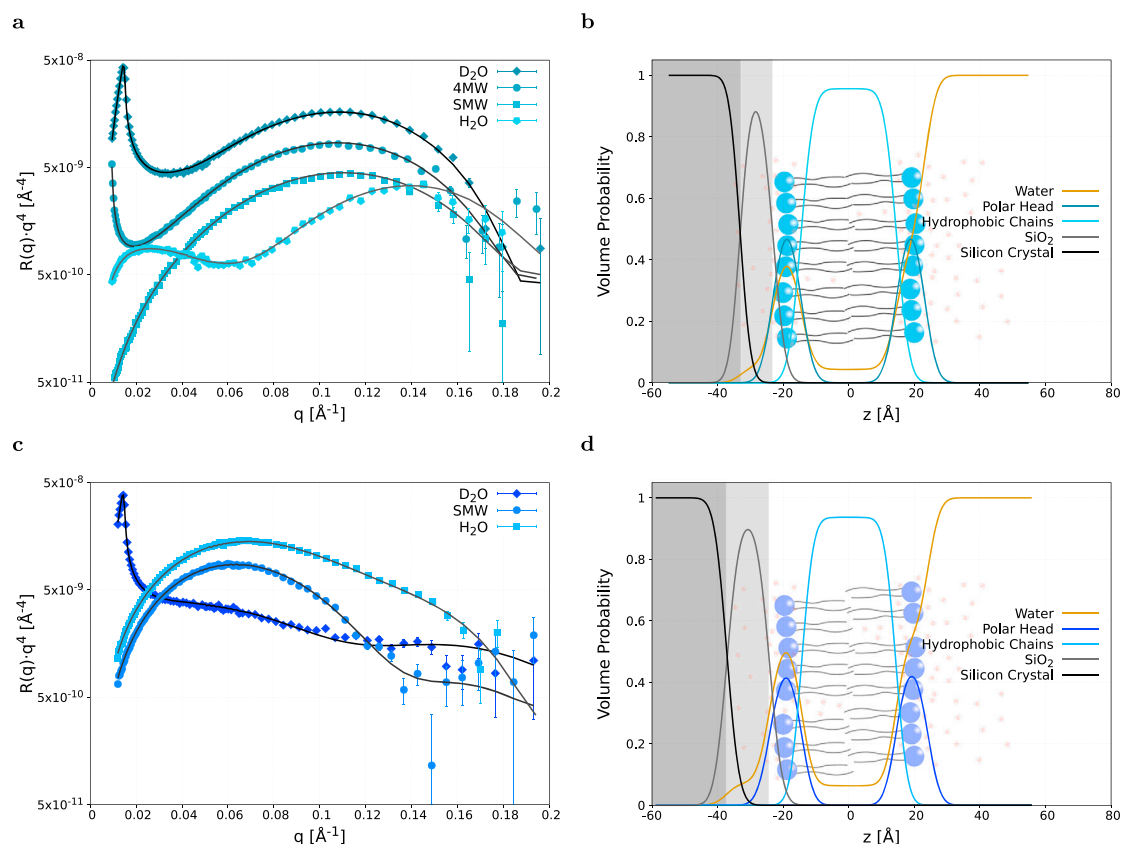

Fig. 5. Structural characterization of PC containing SLBs. (a) and (c) NR experimental data together with the corresponding fitting curves for hPC and dPC, respectively. Volume fraction distribution for the different sample components obtained from the NR data analysis for hPC (b) and dPC (d).

face coverage ($\geq$ 99%). The structural parameters for the hPC/hPG and dPC/dPG-SLBs are reported in Table 2. The obtained values are comparable to those obtained for the PC and PC/PS-SLBs. Interestingly, also in this case, the structure of the hPC/hPG-SLB resulted to be comparable to the dPC/dPG, therefore confirming the low impact of deuteration on the SLB structure, despite the slightly different acyl chain composition between the hydrogenous and deuterated extracts.

SAXS data were collected also on vesicles produced with the hPC/hPG and dPC/dPG mixtures (Fig. 7e). Analysis of the collected curves indicated the formation of unilamellar vesicles with a very similar bilayer structure in case of hPC/hPG compared to dPC/dPG. The structural parameters obtained from the SAXS data analysis are comparable to those obtained by NR (Table 2). SAXS data also confirmed the similar structure exhibited by the PC/PG bilayers compared to PC and PC/PS.
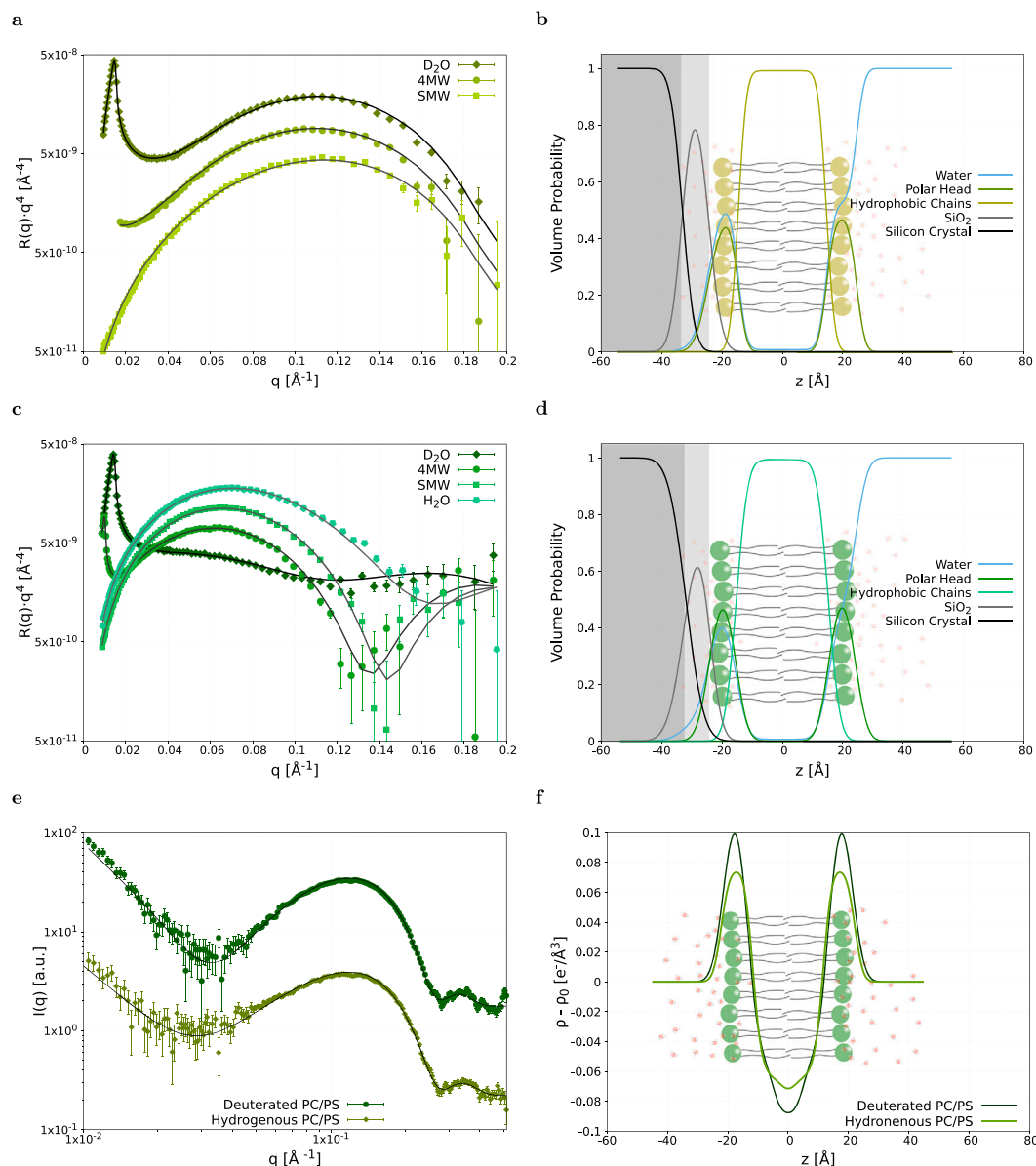
Fig. 6. Structural characterisation of PC/PS bilayers in SLBs and vesicles. (a) and (c) NR experimental data together with the corresponding fitting curves for the hPC/hPS and dPC/dPS mixtures, respectively. The volume fraction distributions for the different sample components were obtained from the NR data analysis for hPC/hPS (b) and dPC/dPS (d). SAXS experimental data for the hPC/hPS and dPC/dPS vesicles (e) and the corresponding scattering length density profiles obtained from data analysis (f).

4. Discussion

Natural lipid extracts are valuable assets for producing more biologically relevant models of cellular membranes. Having access to these lipids both in their hydrogenous and deuterated form enables the design of experiments with techniques such as NMR, NR or infrared spectroscopy, which can be used for a detailed characterisation of the membrane structure and dynamics.

We have previously reported the production and characterisation of hydrogenous and deuterated lipid membranes composed of the total lipid extracts and the GPL mixtures from the yeast *P. pastoris* [22,24,21]. Here, we report an improvised protocol for the purification of the GPL mixtures that includes the use of an HPLC-ELSD setup. This enabled the obtainment of GPL mixtures, that were very pure at significantly high yields. In addition, such an approach allowed for the separation of the GPL mixtures according to the different composition of the polar heads. The compositional analysis of the produced GPL mixtures showed that this purification step by HPLC-ELSD right after the SPE step, was fun-

damental to efficiently remove residual neutral lipids, *e.g.*, sterols and steryl esters.

In this work, we used this optimised purification protocol to produce PC, PS and PG lipid mixtures from *P. pastoris* both in their hydrogenous and deuterated versions. The composition of the acyl chains determined by GC was in agreement with previous results that confirmed the presence of C18 as the predominant species [21], with the monounsaturated C18 chain being more abundant in the deuterated extract compared to the hydrogenous one.

We used the hPC, dPC and mixtures of PC and 20% w/w of either PS or PG (*i.e.*, hPC/hPS, dPC/dPS, hPC/hPG and dPC/dPG) to produce lipid bilayers both in the proximity of a solid substrate (SLBs) or in solution (vesicles). The performed characterisation confirmed the obtainment of high surface coverage SLBs by vesicle fusion at room temperature. Both the structure of the SLBs and the vesicles were in good agreement with each other and indicated that the hydrogenous and deuterated bilayers have a very similar structure and that the addition of PS and PG to PC does not significantly affect the structural parameters. In the case of the
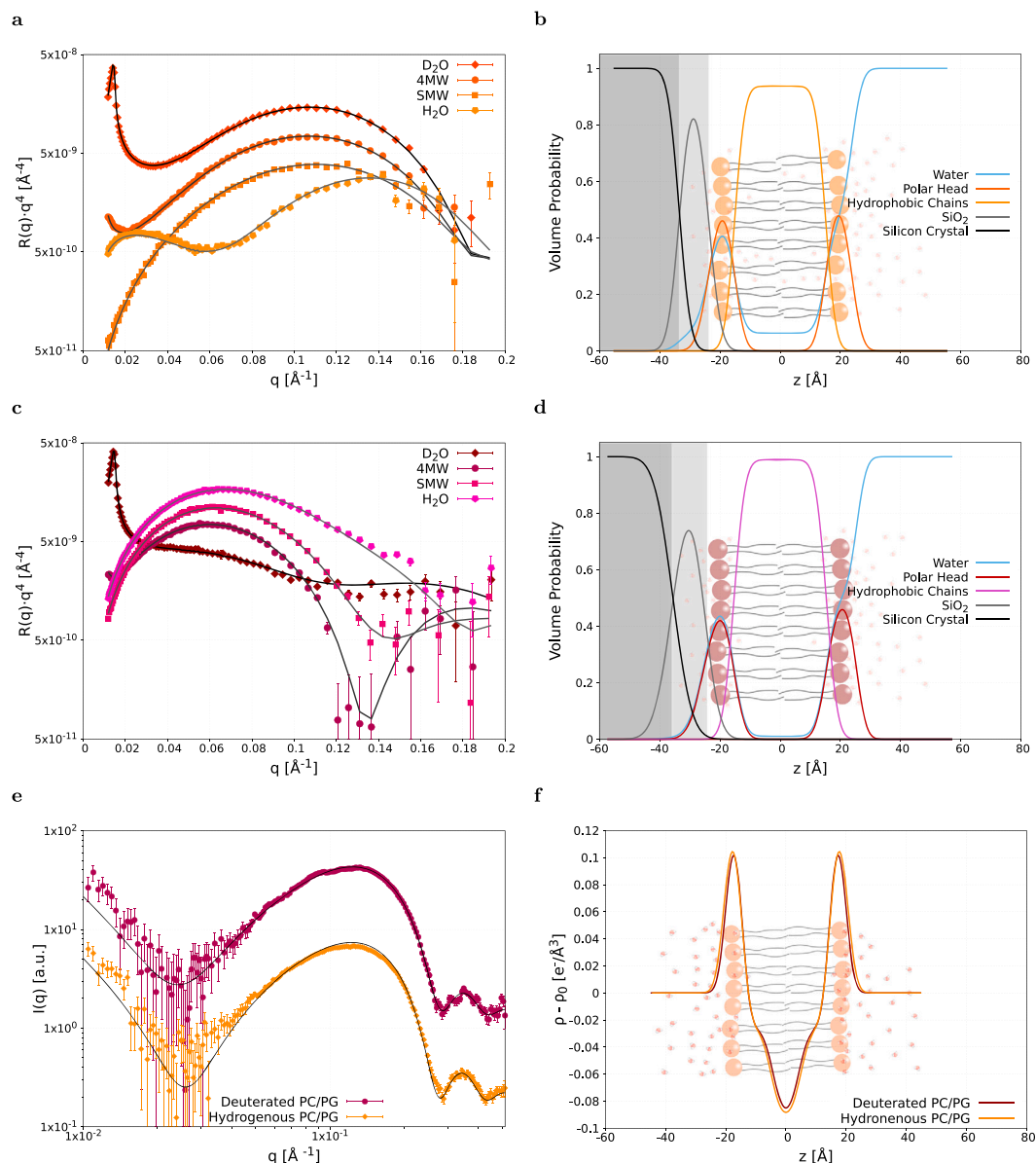
Fig. 7. Structural characterization of PC/PG bilayers in SLBs and vesicles. Structural characterization of PC/PS bilayers in SLBs and vesicles. (a) and (c) NR experimental data together with the corresponding fitting curves for the hPC/hPG and dPC/dPG, respectively. The volume fraction distributions for the different sample components were obtained from the NR data analysis for hPC/hPG (b) and dPC/dPG (d). SAXS experimental data for the hPC/hPG and dPC/dPG vesicles (e) and the corresponding scattering length density profiles obtained from data analysis (f).

deuterated bilayers, we also experimentally determined the deuteration level of the lipids, which resulted to be approximately 95%.

The structure of the PC, PC/PS, PC/PG bilayers resulted to be altogether very similar to that previously reported for pure POPC [25,40], POPC/POPG [41] and POPC/POPS[25] bilayers produced with synthetic GPLs. Nevertheless, despite being structurally similar to the corresponding synthetic analogs, lipid bilayers produced with the *P. pastoris* GPL mixtures, showed a different behaviour when it comes to the interaction with soluble proteins, as recently reported [26]. This different behaviour was hypothesised to be associated to the more complex composition of the acyl chains, which could affect membrane properties other then its structure, e.g. membrane fluidity, lipid lateral diffusion, local lipid dynamics.

In our previous studies [22,24,21,25], we observed that the total GPL extract (containing a mixture of different lipid polar heads and acyl chains) as well as the PC extract produced bilayers with slightly different structural properties depending on whether hydrogenous or deuterated lipids were used. In particular, the deuterated bilayers re-

sulted to be thicker than the hydrogenous ones. We suggested that this difference in structure was the result of the different composition of the acyl chains in the deuterated extracts compared to the hydrogenous one. Indeed, as also reported here, the deuterated extracts exhibit a higher content of monounsaturated C18 chains. However, the characterisation by NR and SAXS discussed in this work, did not highlight the same structural difference between hydrogenous and deuterated bilayers, but instead suggested that deuteration has no significant impact on the bilayer structure, despite the composition of the acyl chain being different in the hydrogenous and deuterated extracts. As mentioned above, the lipid extract characterised in this work were produced with a different protocol including an additional purification step by HPLC-ELSD. The analysis of the HLPC chromatograms (*Supplementary Material* Fig. S1), indicated that without this purification step, the deuterated GPL extract is characterised by a much higher (*approx.* by a factor 1.7) content of neutral lipids, including sterols (which are known to increase membrane thickness) compared to the hydrogenous extract. We therefore suggest, that the previously reported structural differences

Table 2
Bilayer structural parameters obtained from NR and SAXS data analysis: thickness (t), scattering length density (SLD, shown in table as ρ). Surface roughness estimated from NR was in the range of 2-4 Å. * these parameters were not optimised to the experimental data, but calculated according to the GPL mixture composition. ** and *** in the SAXS column are the ρ of the CH_2 and CH_3 respectively. The subscript PH indicates the parameters corresponding to the polar headgroups, whereas CH indicates acyl chains.

PC bilayer		
Parameters	NR	
t_{h-PH} [Å]	9 ± 1	
$\rho_{h-PH} \cdot 10^{-6}$ [Å^{-2}]	1.88*	
t_{h-CH} [Å]	29 ± 1	
$\rho_{h-CH} \cdot 10^{-6}$ [Å^{-2}]	−0.16*	
t_{d-PH} [Å]	10 ± 1	
$\rho_{d-PH} \cdot 10^{-6}$ [Å^{-2}]	7.40 ± 0.05	
t_{d-CH} [Å]	29 ± 1	
$\rho_{d-CH} \cdot 10^{-6}$ [Å^{-2}]	6.60 ± 0.03	

PC/PS bilayer		
Parameters	NR	SAXS
t_{h-PH} [Å]	10 ± 1	10 ± 2
$\rho_{h-PH} \cdot 10^{-6}$ [Å^{-2}]	2.12*	14.9
t_{h-CH} [Å]	29 ± 1	24 ± 2
$\rho_{h-CH} \cdot 10^{-6}$ [Å^{-2}]	−0.17*	8.3**; 4.6***
t_{d-PH} [Å]	9 ± 1	8 ± 2
$\rho_{d-PH} \cdot 10^{-6}$ [Å^{-2}]	7.24 ± 0.03	14.9
t_{d-CH} [Å]	30 ± 1	27 ± 2
$\rho_{d-CH} \cdot 10^{-6}$ [Å^{-2}]	6.53 ± 0.03	8.3**; 4.6***

PC/PG bilayer		
Parameters	NR	SAXS
t_{h-PH} [Å]	9 ± 1	6 ± 2
$\rho_{h-PH} \cdot 10^{-6}$ [Å^{-2}]	2.06*	14.7
t_{h-CH} [Å]	30 ± 1	29 ± 2
$\rho_{h-CH} \cdot 10^{-6}$ [Å^{-2}]	−0.15*	8.3**; 4.6***
t_{d-PH} [Å]	10 ± 1	5 ± 2
$\rho_{d-PH} \cdot 10^{-6}$ [Å^{-2}]	7.39 ± 0.03	14.7
t_{d-CH} [Å]	30 ± 1	29 ± 2
$\rho_{d-CH} \cdot 10^{-6}$ [Å^{-2}]	6.80 ± 0.03	8.3**; 4.6***

between deuterated and hydrogenous bilayers produced with *P. pastoris* lipids were not to ascribe to the larger content of monounsaturated C18 chains, but rather to the higher content of impurities, *i.e.*, neutral lipids, in the deuterated lipid extract compared to the hydrogenous one.

5. Conclusions

Altogether, we report an improved method to produce pure hydrogenous and deuterated GPL extracts from *P. pastoris* in abundant quantities. Further, we show that the GPL extract can also be separated according to the different GPL classes. The developed purification method has a general applicability and it can be extended to other lipid extracts obtained from various cellular systems (such as bacterial or mammalian) without any substantial modification.

We demonstrate that because of the efficient removal of neutral lipids from the investigated extracts, they can be used to produce SLBs by vesicle fusion, as well as lipid monolayers or vesicles at room temperature. In addition, the performed characterisations provide relevant information for future applications of these lipids for producing advanced models of biological membranes to be used as platforms for investigating interactions with biomolecules or drugs.

CRediT authorship contribution statement

KCB (Conceptualisation, Formal analysis, Investigation, Writing-original draft, Project administration); GC (Formal analysis, Investigation, Writing-original draft); AL (Conceptualisation, Writing-original draft); AS (Investigation, Formal Analysis); AM (Investigation, Formal Analysis); MPF (Investigation, Formal Analysis); MT (Investigation, Formal Analysis); VL (Resources); MH (Resources); TS (Investigation); CB (Investigation, Formal Analysis); YYB (Investigation, Formal Analysis); AM (Investigation); LP (Investigation, Writing-review & editing); GF (Conceptualisation, Investigation, Project administration, Funding, Writing-review & editing).

Declaration of competing interest

The authors declare that they have no known competing financial interests or personal relationships that could have appeared to influence the work reported in this paper.

Data availability

Data will be made available on request.

Appendix A. Supplementary material

Supplementary material related to this article can be found online at https://doi.org/10.1016/j.jcis.2023.04.135.

References

[1] T. Harayama, H. Riezman, Understanding the diversity of membrane lipid composition, Nat. Rev. Mol. Cell Biol. 19 (2018) 281–296, https://doi.org/10.1038/nrm.2017.138.

[2] G. van Meer, A.I.P.M. de Kroon, Lipid map of the mammalian cell, J. Cell Sci. 124 (1) (2011) 5–8, https://doi.org/10.1242/jcs.071233.

[3] A. Shevchenko, K. Simons, Lipidomics: coming to grips with lipid diversity, Nat. Rev. Mol. Cell Biol. 11 (2011) 593–598, https://doi.org/10.1038/nrm2934.

[4] A.M. Seddon, P. Curnow, P.J. Booth, Membrane proteins, lipids and detergents: not just a soap opera, in: Lipid-Protein Interactions, Biochim. Biophys. Acta, Biomembr. 1666 (1) (2004) 105–117, https://doi.org/10.1016/j.bbamem.2004.04.011.

[5] A. Luchini, G. Vitiello, Mimicking the mammalian plasma membrane: an overview of lipid membrane models for biophysical studies, Biomimetics 6 (1) (2021), https://doi.org/10.3390/biomimetics6010003.

[6] G.J. Hardy, R. Nayak, S. Zauscher, Model cell membranes: techniques to form complex biomimetic supported lipid bilayers via vesicle fusion, Curr. Opin. Colloid Interface Sci. 18 (5) (2013) 448–458, https://doi.org/10.1016/j.cocis.2013.06.004.

[7] L.A. Bagatolli, J.H. Ipsen, A.C. Simonsen, O.G. Mouritsen, An outlook on organization of lipids in membranes: searching for a realistic connection with the organization of biological membranes, Prog. Lipid Res. 49 (4) (2010) 378–389, https://doi.org/10.1016/j.plipres.2010.05.001.

[8] G. Fragneto, R. Delhom, L. Joly, E. Scoppola, Neutrons and model membranes: moving towards complexity, Curr. Opin. Colloid Interface Sci. 38 (2018) 108–121, https://doi.org/10.1016/j.cocis.2018.10.003.

[9] T.K. Lind, H. Wacklin, J. Schiller, M. Moulin, M. Haertlein, T.G. Pomorski, M. Cárdenas, Formation and characterization of supported lipid bilayers composed of hydrogenated and deuterated escherichia coli lipids, PLoS ONE 10 (2015) 1–16, https://doi.org/10.1371/journal.pone.0144671.

[10] S. Himbert, R.J. Alsop, M. Rose, L. Hertz, A. Dhaliwal, J.M. Moran-Mirabal, C.P. Verschoor, D.M.E. Bowdish, L. Kaestner, C. Wagner, M.C. Rheinstädter, The molecular structure of human red blood cell membranes from highly oriented, solid supported multi-lamellar membranes, Sci. Rep. 7 (2017) 39661, https://doi.org/10.1038/srep39661.

[11] O. Dunne, M. Weidenhaupt, P. Callow, A. Martel, M. Moulin, S.J. Perkins, M. Haertlein, V. Forsyth, Matchout deuterium labelling of proteins for small-angle neutron scattering studies using prokaryotic and eukaryotic expression systems and high cell-density cultures, Eur. Biophys. J. 46 (2017) 425–432, https://doi.org/10.1007/s00249-016-1186-2.

[12] M. Haertlein, M. Moulin, J.M. Devos, V. Laux, O. Dunne, V. Trevor Forsyth, Chapter five - biomolecular deuteration for neutron structural biology and dynamics, in: Z. Kelman (Ed.), Isotope Labeling of Biomolecules - Applications, in: Methods in Enzymology, vol. 566, Academic Press, 2016, pp. 113–157.

[13] O. Dunne, M. Weidenhaupt, P. Callow, A. Martel, M. Moulin, S.J. Perkins, M. Haertlein, V. Forsyth, Fractional deuteration applied to biomolecular solid-state nmr spectroscopy, J. Biomol. NMR 52 (2012) 91–101, https://doi.org/10.1007/s10858-011-9585-2.

[14] S.A. Tatulian, Structural Characterization of Membrane Proteins and Peptides by FTIR and ATR-FTIR Spectroscopy, Humana Press, Totowa, NJ, 2013, pp. 177–218.

[15] N.R. Yepuri, T.A. Darwish, A.M. Krause-Heuer, A.E. Leung, R. Delhom, H.P. Wacklin, P.J. Holden, Synthesis of perdeuterated 1-palmitoyl-2-oleoyl-sn-glycero-3-phosphocholine ([d82]popc) and characterisation of its lipid bilayer membrane structure by neutron reflectometry, ChemPlusChem 81 (3) (2016) 315–321, https://doi.org/10.1002/cplu.201500452.

[16] M. Moulin, G.A. Strohmeier, M. Hirz, K.C. Thompson, A.R. Rennie, R.A. Campbell, H. Pichler, S. Maric, V.T. Forsyth, M. Haertlein, Perdeuteration of cholesterol for neutron scattering applications using recombinant pichia pastoris, Chem. Phys. Lipids 212 (2018) 80–87, https://doi.org/10.1016/j.chemphyslip.2018.01.006.

[17] A. de Ghellinck, H. Schaller, V. Laux, M. Haertlein, M. Sferrazza, E. Maréchal, H. Wacklin, J. Jouhet, G. Fragneto, Production and analysis of perdeuterated lipids from pichia pastoris cells, PLoS ONE 9 (4) (2014) e92999.

[18] S. Haon, S. Augé, M. Tropis, A. Milon, N.D. Lindley, Low cost production of perdeuterated biomass using methylotrophic yeasts, J. Labelled Compd. Radiopharm. 33 (11) (1993) 1053–1063, https://doi.org/10.1002/jlcr.2580331108.

[19] S. Massou, S. Augé, M. Tropis, N.D. Lindley, A. Milon, Nmr analyses of deuterated phospholipids isolated from pichia angusta, J. Chim. Phys. 95 (2) (1998) 406–411, https://doi.org/10.1051/jcp:1998152.

[20] K. Grillitsch, P. Tarazona, L. Klug, T. Wriessnegger, G. Zellnig, E. Leitner, I. Feussner, G. Daum, Isolation and characterization of the plasma membrane from the yeast pichia pastoris, Biochim. Biophys. Acta 1838 (2014) 1889–1897.

[21] A. de Ghellinck, G. Fragneto, V. Laux, M. Haertlein, J. Jouhet, M. Sferrazza, H. Wacklin, Lipid polyunsaturation determines the extent of membrane structural changes induced by amphotericin b in pichia pastoris yeast, Biochim. Biophys. Acta, Biomembr. 1848 (10 Part A) (2015) 2317–2325, https://doi.org/10.1016/j.bbamem.2015.06.006.

[22] A. Luchini, R. Delhom, B. Demé, V. Laux, M. Moulin, M. Haertlein, H. Pichler, G.A. Strohmeier, H. Wacklin, G. Fragneto, The impact of deuteration on natural and synthetic lipids: a neutron diffraction study, Colloids Surf. B, Biointerfaces 168 (2018) 126–133, https://doi.org/10.1016/j.colsurfb.2018.02.009.

[23] A. Luchini, R. Delhom, V. Cristiglio, W. Knecht, H. Wacklin-Knecht, G. Fragneto, Effect of ergosterol on the interlamellar spacing of deuterated yeast phospholipid multilayers, Chem. Phys. Lipids 227 (2020) 104873, https://doi.org/10.1016/j.chemphyslip.2020.104873.

[24] A. Luchini, G. Corucci, K. Chaithanya Batchu, V. Laux, M. Haertlein, V. Cristiglio, G. Fragneto, Structural characterization of natural yeast phosphatidylcholine and bacterial phosphatidylglycerol lipid multilayers by neutron diffraction, Front. Chem. 9 (2021), https://doi.org/10.3389/fchem.2021.628186.

[25] A. Luchini, F. Sebastiani, F.G. Tidemand, K.C. Batchu, M. Campana, G. Fragneto, M. Cárdenas, L. Arleth, Peptide discs as precursors of biologically relevant supported lipid bilayers, J. Colloid Interface Sci. 585 (2021) 376–385, https://doi.org/10.1016/j.jcis.2020.11.086.

[26] A. Luchini, S. Micciulla, G. Corucci, K.C. Batchu, A. Santamaria, V. Laux, T. Darwish, R.A. Russell, M. Thepaut, I. Bally, F. Fieschi, G. Fragneto, Lipid bilayer degradation induced by Sars-cov-2 spike protein as revealed by neutron reflectometry, Sci. Rep. 11 (2021) 14867, https://doi.org/10.1038/s41598-021-93996-x.

[27] Y. Gerelli, A. de Ghellinck, J. Jouhet, V. Laux, M. Haertlein, G. Fragneto, Multilamellar organization of fully deuterated lipid extracts of yeast membranes, Acta Crystallogr., Sect. D 70 (12) (2014) 3167–3176, https://doi.org/10.1107/S1399004714022913.

[28] E.G. Bligh, W.J. Dyer, A rapid method of total lipid extraction and purification, Can. J. Biochem. Physiol. 37 (8) (1959) 911–917.

[29] S. Amiar, J.I. MacRae, D.L. Callahan, D. Dubois, G.G. van Dooren, M.J. Shears, M.-F. Cesbron-Delauw, E. Maréchal, M.J. McConville, G.I. McFadden, et al., Apicoplast-localized lysophosphatidic acid precursor assembly is required for bulk phospholipid synthesis in toxoplasma gondii and relies on an algal/plant-like glycerol 3-phosphate acyltransferase, PLoS Pathog. 12 (8) (2016) e1005765.

[30] S. Ramakrishnan, M.D. Docampo, J.I. MacRae, F.M. Pujol, C.F. Brooks, G.G. Van Dooren, J.K. Hiltunen, A.J. Kastaniotis, M.J. McConville, B. Striepen, Apicoplast and endoplasmic reticulum cooperate in fatty acid biosynthesis in apicomplexan parasite toxoplasma gondii, J. Biol. Chem. 287 (7) (2012) 4957–4971.

[31] R. Campbell, H. Wacklin, I. Sutton, R. Cubitt, G. Fragneto, The new horizontal neutron reflectometer at the ill, Eur. Phys. J. Plus 125 (2011) 107, https://doi.org/10.1140/epjp/i2011-11107-8.

[32] P. Gutfreund, T. Saerbeck, M.A. Gonzalez, E. Pellegrini, M. Laver, C. Dewhurst, R. Cubitt, Towards generalized data reduction on a chopper-based time-of-flight neutron reflectometer, J. Appl. Crystallogr. 51 (3) (2018) 606–615, https://doi.org/10.1107/S160057671800448X.

[33] J.F. Nagle, R.M. Venable, E. Maroclo-Kemmerling, S. Tristram-Nagle, P.E. Harper, R.W. Pastor, Revisiting volumes of lipid components in bilayers, J. Phys. Chem. B 123 (12) (2019) 2697–2709.

[34] L.G. Parratt, Surface studies of solids by total reflection of x-rays, Phys. Rev. 95 (2) (1954) 359.

[35] P. Pernot, M. Brennich, M. Tully, The rise of biosaxs at the esrf: Bm29 beamline for saxs on proteins in solution, Acta Crystallogr. Sect. A Found. Adv. 74 (2018) a7.

[36] N. Kucerka, J. Pencer, J.N. Sachs, J.F. Nagle, J. Katsaras, Curvature effect on the structure of phospholipid bilayers, Langmuir 23 (3) (2007) 1292–1299.

[37] M.P. Frewein, M. Doktorova, F.A. Heberle, H.L. Scott, E.F. Semeraro, L. Porcar, G. Pabst, Structure and interdigitation of chain-asymmetric phosphatidylcholines and milk sphingomyelin in the fluid phase, Symmetry 13 (8) (2021) 1441.

[38] P. Virtanen, et al., SciPy 1.0: fundamental algorithms for scientific computing in Python, Nat. Methods 17 (3) (2020) 261–272, https://doi.org/10.1038/s41592-019-0686-2.

[39] A. Dickey, R. Faller, Examining the contributions of lipid shape and headgroup charge on bilayer behavior, Biophys. J. 95 (6) (2008) 2636–2646, https://doi.org/10.1529/biophysj.107.128074.

[40] A. Luchini, Y. Gerelli, Applications of neutron reflectometry in biology, EPJ Web Conf. 236 (2020) 04002, https://doi.org/10.1051/epjconf/202023604002.

[41] A. Luchini, Y. Gerelli, G. Fragneto, T. Nylander, G.K. Pálsson, M.-S. Appavou, L. Paduano, Neutron reflectometry reveals the interaction between functionalized spions and the surface of lipid bilayers, Colloids Surf. B, Biointerfaces 151 (2017) 76–87, https://doi.org/10.1016/j.colsurfb.2016.12.005.